A Numerical Study of Deep Borehole Heat Exchangers Efficiency in Unconventional Geothermal Settings

Theo Renaud[1*], Patrick Verdin[1], Gioia Falcone[2]

[1] Energy and Power, Cranfield University, Cranfield, MK43 0AL, UK

[2] School of Engineering, University of Glasgow, Glasgow G12 8QQ, UK

* theo.renaud@cranfield.ac.uk

Keywords: Deep Borehole Heat Exchangers, Numerical simulation, CFD

ABSTRACT

The geothermal energy industry is facing several challenges related to heat recovery efficiency and economic feasibility. Research on superheated and supercritical geothermal systems is progressing in Europe, triggered by the Iceland Deep Drilling project (IDDP) and the DESCRAMBLE project in Italy. In Iceland, the IDDP-1 well, which reached a magma intrusion at a depth of 2100 m, raised new opportunities to untap the geothermal potential near shallow magmatic intrusions.

Given their highly corrosive nature, geothermal fluids weaken the wellbore's integrity during conventional geothermal production. Closed-loop Deep Borehole Heat Exchangers (DBHE) that do not require fluid exchange between the subsurface and the wells represent a strategic alternative for recovering heat from these unconventional geothermal resources, while minimizing the risk of in-situ reservoir damage.

The thermal influence and heat recovery associated with a hypothetical DBHE drilled into the IDDP geological site, were investigated via Computational Fluid Dynamics (CFD), simulating 30 years of production. Two wellbore designs were considered, based on simplified geological properties from the IDDP-1 well description.

The results show that, during the first year of production, the output temperature is function of the working fluid velocity before reaching pseudo-steady state conditions. The cooling perturbation near the bottom hole is shown to grow radially from 10 to 40 m between 1 and 10 years of production, and the output power calculated reaches up to 1.2 MW_{th} for a single well. Based on assumptions on well-well distance, the predicted output from a single DBHE is then extrapolated to field scale for comparison with the short-term flow potential shown by the original IDDP-1 well. The significantly lower technical risks of a closed-loop DBHE system might outweigh the lower thermal output per well; this is however subject to full economic analysis.

1. INTRODUCTION

Geothermal energy is considered as a sustainable energy to use in order to decrease dependency on fossil fuels (Fuss et al. 2008). In Europe, the European Geothermal Energy Council (EGEC) identified a total installed geothermal electricity capacity of about 2.8 GWe, generated from 117 power plants in 2017.

While Enhanced Geothermal Systems (EGS) are limited due to technological issues, notably seismicity-induced (Grigoli. et al. 2018), closed-loop single-wells can offer alternative solutions to extract underground thermal energy. Borehole Heat Exchanger (BHE) or Deep Borehole Heat Exchangers (DBHE) aim to extract geothermal energy by circulating a working fluid in a well without producing geofluids or requesting injection processes. Alimonti et al. (2018) reviewed the technical investigations of DBHE for converting oil and gas wells into geothermal ones. The application of DBHE worldwide is currently investigated for a maximum depth-use of 3 km for potentially generating 0.15-2.5 MW_{th} thermal power and 0.25 - 364 MW_e electrical power.

Several DBHEs exist in Switzerland and Germany, up to a depth of 2.7 km for heat pump systems (Dijkshoorn et al. 2013, Kohl et al. 2002). DBHE in Weissbad (Switzerland) reaches a temperature T=45°C at 1213 m (Figure 1). DBHE systems were considered to retrofit abandoned oil wells (Kujawa et al. 2006, Caulk and Tomac 2017) with various working fluids such as isobutane at supercritical state (Cheng et al. 2013) or water (Alimonti and Soldo 2016). Several cases from 25°C/km and 50°C/km and between 2-6 km were investigated, giving variable potential output energy. With 50°C/km, the output power efficiency starts to be significant below 3 km. Injection temperatures, thermal gradients, flow rates and the insulation of the inner pipe appeared to be the main parameters ensuring an efficient thermal recovery. The well diameter affects the residence time of the fluid.

Research on superheated/supercritical geothermal systems is occurring in Europe, notably triggered by the DESCRAMBLE project (Bertani et al. 2018) in Italy and the Iceland Deep Drilling project (IDDP) (Frideifsson et al. 2015). The IDDP-1 well in Krafla raised challenges to assess the geothermal potential near the magma. The well was stopped at a depth of

2072 m after drilling into the magma, between 2092 m and 2104 m (Palsson et al. 2014). The wellhead temperature reached 450°C with a superheated steam at 140 bars. Axelsson et al. (2014) estimated the existence of a 30-50 m thick conductive layer above the magmatic intrusion.

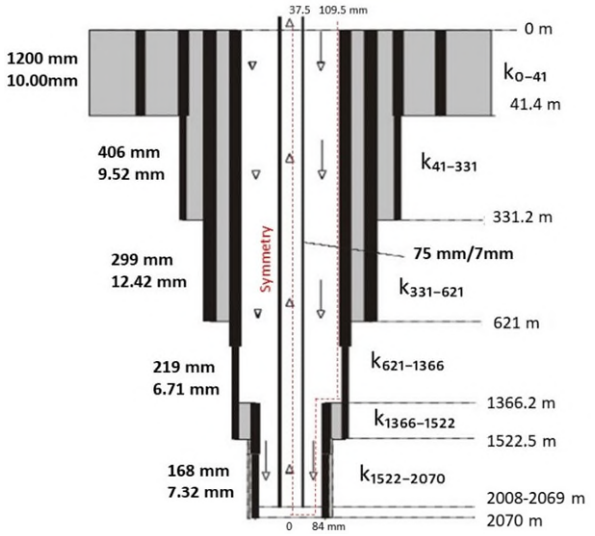

Figure 1: Deep Borehole exchanger in Weissbad; geometry used and effective thermal conductivities of the external wall (from Kohl et al. 2000). The red dash line describes the axisymmetric model with its effective thermal conductivity *k* (Table 4).

DBHEs are conventionally investigated for low-medium temperatures and only one experimental study from Morita et al. (1992), dealt with high temperature conditions around 110°C at a depth of 876.5 m, in Hawaii(Morita et al. 1992). As there is no contact between geofluids and the working fluid, DBHEs can bypass the aggressive upflow present in very hot geothermal reservoirs by directly targeting the available heat. Despite a low efficiency compared to open-loop EGS, DBHEs have not yet been investigated in more favourable areas, such as under the recently discovered superheated-supercritical conditions (Falcone et al. 2018).

In this study, the energy production from a single-well design applied to the Krafla very hot environment is investigated.

2. THE CLOSED-LOOP MODEL

2.1 Geometry and boundary conditions

1D analytical calculations of the borehole fluid flow and heat transfer (Holmberg et al. 2016, Kolo et al. 2014) or full 3D numerical Computational Fluid Dynamics (CFD) simulations (Huang et al. 2015, Noorollahi et al. 2015) were used to model closed-loop single wells. The present work uses an axisymmetric-based approach, reducing the 3D description to a 2D CFD model.

Figure 1 shows the single well design investigated, for which the settings of the Weissbad BHE extended from 1213.30 m to 2070 m (depth reached by the IDDP-1 well) are applied. The cement and casing properties are both extracted from Kohl et al. (2000). The flow circulates downward in the external annulus of the well and the temperature increases with depth. From the bottom of the well, the heated fluid flows to the surface via the internal pipe. Liquid water with constant properties listed in Table 4is used as working fluid. No phase change is assumed.

An axisymmetric domain extended to 200 m radially is built to avoid any influence of the boundary temperature on the well. The Krafla volcanic system on the IDDP-1 well can be simplified by considering three distinct zones, as shown in Figure 2, with properties provided in Table 4. The cylindrical area outside the DBHE is made of basalt with constant material properties. A 50 m thick conductive layer (Zone 3) separates the porous Zone 2 (similar to the reservoir) from the magma region located at a depth of 2140 m. This insulated layer is set with a lower thermal conductivity value.

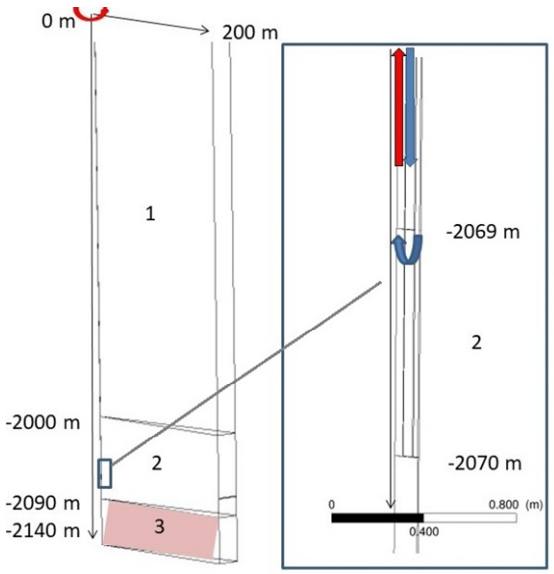

Figure 2: Scheme of the axisymmetric DBHE model, including the three porous zones detailed in Appendix A. The right picture is a detail of the bottom hole - Design 2.

The walls of the well are defined with a constant 7 mm thickness whose effective thermal conductivity k_{eff} and specific heat c vary (Table 4). These variations correspond to the different casing and cement thickness sections in the Weissbad BHE (Figure 1). The heat conduction across the well bore is only considered as the CFD code solves a 1D steady equation at the wall to compute the thermal resistance, Δx is the wall thickness (ANSYS 2011).

The water enters into the annular space with an initial velocity and a constant temperature. The outlet of the well is set with a pressure outlet boundary condition. A pressure atmospheric condition of 1 bar and 10°C is applied at the surface of the porous model. The bottom boundary of the model is set with a constant temperature of 650°C. The side boundary of the model

is considered adiabatic. Two designs are investigated: Design 1 applies the same proportion between the lengths of the casing sections as the Weissbad BHE, while Design 2 extends the inner well up to 1 m above the bottom hole.

2.2 Mathematical description

The CFD code ANSYS Fluent 17.1.0 is used to solve the mass conservation, momentum and energy equations for water. It is based on the finite volume approximation. Ignoring the convective acceleration and diffusion, the pressure in the porous medium is reduced to the Darcy's law (ANSYS 2016):

$$\nabla p = -\frac{\mu}{\alpha}\vec{v} \qquad [1]$$

where p is the pressure [Pa], α is the permeability [m^2], μ the viscosity [Pa.s], and v the velocity [m/s].
The continuity equation in the axisymmetric grid is written as:

$$\frac{\partial \rho}{\partial t} + \frac{\partial(\rho v_x)}{\partial r} + \frac{\partial(\rho v_r)}{\partial r} + \frac{\rho v_r}{r} = 0 \qquad [2]$$

The radial r and axial x momentum in an axisymmetric model are described in Table 5.
The energy equation can be written as:

$$\frac{\partial(\rho E)}{\partial t} + \nabla.(\vec{v}(\rho E + p)) = \nabla.(k_{eff}\nabla T - \sum_j h_j \vec{J}_j + (\overline{\overline{\tau_{eff}}}.\vec{v})) \qquad [7]$$

where k_{eff} is the effective thermal conductivity [W/m.K] and T the temperature [K]. The two right hand side terms describe diffusion and viscous dissipations terms. E is the energy calculated as follow:

$$E = \int_T^{Tref} c\, dT + \frac{p}{\rho} + \frac{v^2}{2} \qquad [8]$$

where c is the heat capacity [J/kg.K].

Simulation settings and models used in the CFD study are listed in Table 1.

Table 1: Numerical parameters considered in the CFD model (ANSYS 2016).

Turbulence model	realizable k-ε
Coupling velocity & pressure	PISO algorithm
Pressure discretization	PRESTO scheme
Discretization scheme	Second order
Residuals convergence criteria	10^{-6}.
Time step	1 s – 2h

2.3 Initial conditions

Up to 2 km, the temperature gradient is extracted from the data log measurements (Frideifsson et al. 2015) and implemented in the CFD flow solver via an user-defined function (UDF). The bottom hole conditions in the IDDP-1 well were previously studied as temperature log measurements did not reach the bottom hole depth.

The estimates appeared to be in the range 390°C-400°C (Axelsson et al. 2014), potentially reaching 450°C (Scott et al. 2015). The latter temperature values were measured during a discharge test, suggesting the potential existence of higher temperatures due to water recharge circulation (Axelsson et al. 2014, Ingason et al. 2014).
Below 2 km, pressure and temperature distributions are calculated under steady-state conditions see Figure 3.

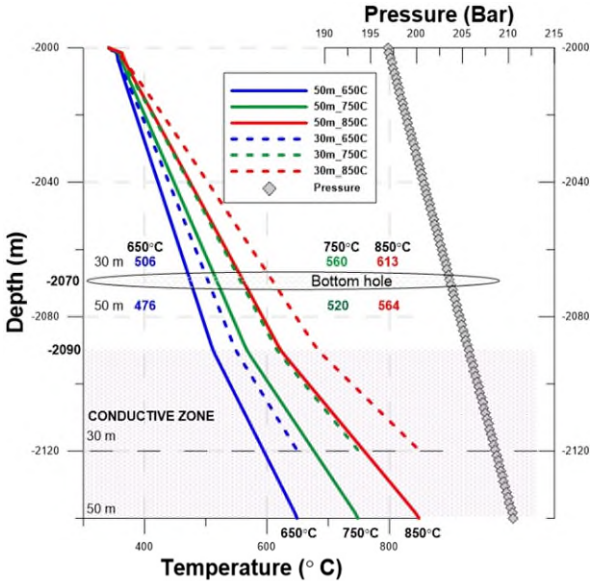

Figure 3: Steady-state calculation of the initial temperature and pressure distributions below 2 km, based on the thickness of the conductive layer and the bottom temperature.

The only bottom hole temperature below 500°C is obtained with a 50 m conductive layer thickness above an intrusion at a temperature of 650°C, a simulated magmatic temperature below the published estimates at 2.1 km (Axelsson et al. 2014). The thermal conductivity of the insulated layer could be lowered, as studies invoke the existence of a very low conductivity layer (Schiffman et al. 2014). Thus, the latter configuration is selected, to keep a relevant thermal distribution near the bottom hole.

3. MESH INDEPENDENCE STUDY

To insure that numerical results do not depend of the mesh density, a mesh-independence study is carried out. Meshes composed of hexahedral cells with local refinements from 0.1 mm to 1 m, are generated with the pre-processor ICEM CFD 17.1.0. Figure 4 shows the temperature outlet and the radial values of turbulence kinetic energy in the well, below the internal pipe, at a depth of 2008.1 m, obtained with four meshes comprising 102 000, 313 200, 418 000 and 664 720 cells, for Design 1.

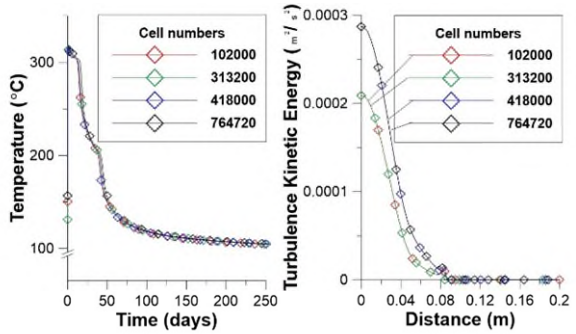

Figure 4: Transient outlet temperature (left) and radial turbulence kinetic energy (right) at 2008.1 m, with different meshes - Design 1.

When looking at the turbulence kinetic energy, there is no significant difference between the simulated results obtained with the two finer meshes. The mesh comprising 418 000 cells is therefore selected for the rest of the study.

Note that the number of iterations per time-step chosen by the user can affect the results at the start of the simulation, see Figure 5. It appears clearly that the default number of iterations per time-step in Fluent (20) is too low to provide accurate results. Results obtained with the default value diverge significantly from the values obtained when 60-100 iterations per time-step are applied, for which a convergence of the temperature distribution is obtained. 80 iterations per time-step are therefore applied for this numerical work. Using these settings, results converge to a pseudo-equilibrium state after 60 days.

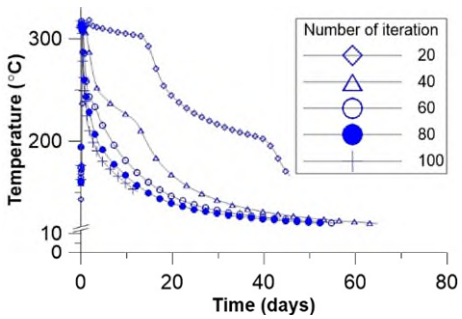

Figure 5: Outlet temperature over time based on the iterations per time step - Design 1.

4. RESULTS

4.1 Thermal recovery

Figure 6 shows the outlet temperature for different injection velocities and for an injection temperature of 10°C. Very high temperatures are visible at the start of the simulation; this agrees with the temperatures obtained during the discharge test (Palsson et al. 2014). Later on, a sharp temperature decrease appears. The system then generates a short-time transitional behavior until pseudo-equilibrium is reached.

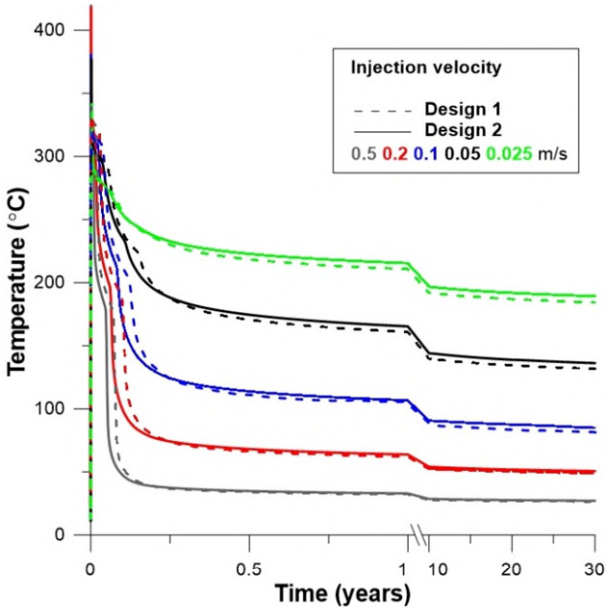

Figure 6: Production temperature over time, based on the injection velocity, until 30 years of simulation.

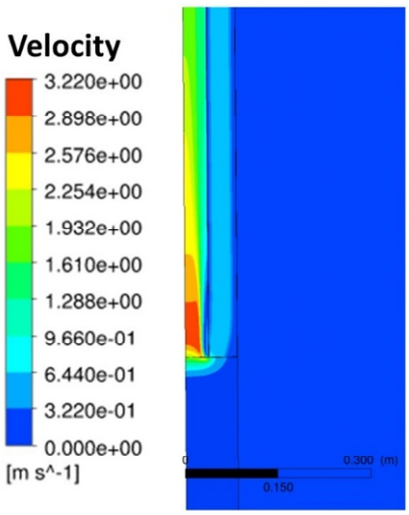

Figure 7: Velocity profile at the bottom of the well - Design 2 (2069 m).

The velocity distribution around the bottom of the well is presented in Figure 7. When the fluid reaches the bottom, the water flows directly towards the top without reaching the bottom end (2070 m), which is a no circulation zone. Thus, the heat recovered with Design 2 is improved as the inner well is deeper than for to Design 1. As seen in Figure 6, the output temperature is enhanced by a factor of 2.5-3.0 %.

4.2 Thermal influence

The heat extraction induces radial temperature changes at the bottom hole. Figure 8 shows the horizontal temperature distribution at 2070 m, based on the injection velocity. Design 2 only affects the bottom hole radial environment. This cooling effect is higher if the injection velocity is high, e.g. associated with a higher heat exchange.

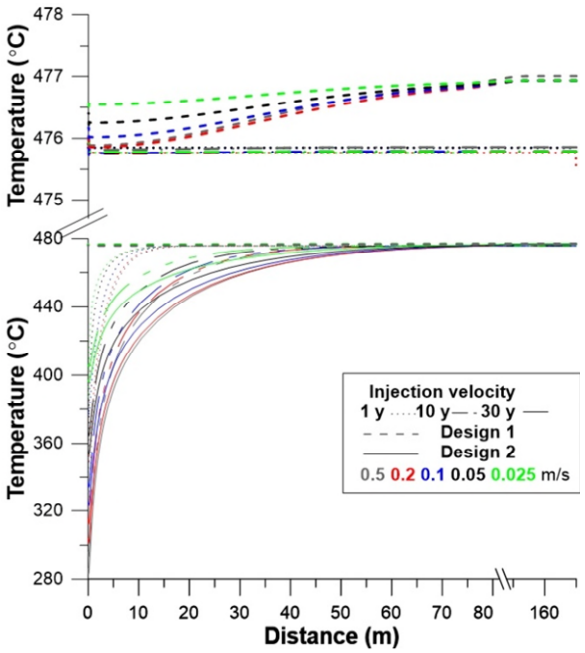

Figure 8: Radial temperature distribution at 2070 m after 10 years for Designs 1 and 2. The top graph is a narrower range of temperature for Design 1.

The steady reservoir temperature is obtained 15 m far (radial distance) from the well centre after 1 year, 40-45 m far after 10 years and extend to 80 m after 30 years.

4.3 Power generation

The thermal and electric powers from an Organic Rankine Cycle Power plant (calculation methodology described in Alimonti and Soldo, 2016), is presented in Table 2, after a 30 year simulated period.

Table 2: Thermal power and Electric power generated in an ORC plant based on the injection velocities and temperature.

v [m/s]	T_{inj} [C°]	10	20	40	60
0.025	kW_{th}	590.0	550.9	520.4	494.0
	kW_e	**90.6**	**86.44**	84.88	86.56
0.05	kW_{th}	847.4	812.5	742.7	673.7
	kW_e	**88.12**	**88.45**	88	86.32
0.1	kW_{th}	1019	975.	888	803
	kW_e	57.04	60.95	67.25	71.36
0.2	kW_{th}	1116	1085	984.0	887.1
	kW_e	26.73	35.02	47.12	56.33
0.5	kW_{th}	**1179**	**1120**	1021.	918.0
	kW_e	2.4	11.96	28.67	41.73

The calculated thermal power reaches nearly 1.2 MW_{th} considering an injection velocity of 0.5 m/s and an injection temperature of 10-20°C. Globally, the overall thermal power production is lowered when the injection temperature increases. On the contrary, high injection velocities and low injection temperatures lower the electric power values. The best-case scenario for electricity production using an ORC cycle is for an injection velocity of 0.05 m/s or 0.025 m/s, reaching up to 90 kW_e. Otherwise, a direct-use of the heat is more efficient using high injection velocities. These figures also demonstrate that the heat recovery using pulsating cycles in shorter periods of time, might generate much more energy.

4.4 Comparison with published studies

Unfortunately, no measurements are available to compare with the simulated results obtained in this work. Only the initial pressure and temperature in the IDDP-1 well are available. Other simulated results from the literature for closed-loop systems are however presented in Table 3, to provide some sort of comparison. Alimonti and Soldo (2016) claim a 45% efficiency decrease after 5 years, giving a corrected output of 675 kW_{th} and 60.3 kW_e. Bu et al. (2012) conclude on a similar range of output power, with a smaller borehole length, compensated by the higher geothermal gradient. The power calculation includes a flash-steam power plant in Bu et al. (2012) whereas an ORC power plant is considered by Alimonti and Soldo (2016). The present study, performed with a very hot geothermal gradient, shows higher extracted energy values; this is in agreement with available information from the literature.

Table 3: Results from published numerical simulations compared to the present study

	Alimonti and Soldo (2016)	Bu et al. (2012)	Present study
Depth [m]	6000	4000	2070
°C/km	26	45	>200
Time [years]	-	10	30
T_{out}	132.5	129.8	27.6-205.9
kW_{th}	1500	815.7	494-1179
kW_e	134	53.7	2.39-90.59

5. CONCLUSION

A DBHE numerical model was developed, and transient simulations close to a magmatic intrusion, based on the Iceland IDDP-1 well conditions, were performed. Two designs derived from the BHE completion in Weissbad were considered in this work.
The unsteady well bore temperatures gave output temperatures constrained by the injection velocity and injection temperature. Three thermal stage behaviours were observed: i.) early high temperature recovery, ii.) rapid transitional stage and iii.) pseudo-steady state. It was shown that the heat recovery could be improved by 2.5-3% when using a deeper inner pipe, close to the downhole depth.
The bottom hole surroundings were shown to cool-down, up to 80 m after 30 years. The best case scenario

for a single well was obtained for an injection velocity of 0.025-0.05 m/s, reaching about 90 kW_e after 30 years. This environment could provide more energy to single-well systems but would remain limited to electricity production. Nevertheless, the low technical risks associated with DBHEs are attractive in a very hot environment and could justify a full economic analysis. Assuming similar underground conditions in a 300 m area surrounding the IDDP-1 well, it is estimated that four additional hypothetical single-wells could generate less than 500 kW_e but up to 6 MW_{th} in the long-term. This is low compared to estimates from expected short term supercritical direct production (35 MW_e), but not to be dis-regarded as DBHEs are safer to run and maintain. The pulsating use of single-wells might offer interesting perspectives to obtain a reliable source of energy. Additional work should however be performed, considering phase-change, and a potential inclusion of thermosiphon effects.

Acknowledgements

This research is supported by the UK Engineering and Physical Sciences Research Council (EPSRC) [Project reference 1878602].

6 .REFERENCES

Alimonti, C., and Soldo, E.: Study of Geothermal Power Generation from a Very Deep Oil Well with a Wellbore Heat Exchanger, *Renewable Energy*, 86, (2016), 292–301.

Alimonti, C., Soldo, E., Bocchetti, D. and Berardi, D. The Wellbore Heat Exchangers: A Technical Review, *Renewable Energy* 123, (2018), 353–81.

ANSYS FLUENT User's Guide, (2011).

ANSYS FLUENT Theory Guide, 17, (2016).

Axelsson, G., Thorsteinn E., and Sigrídur S. G.: Modelling of Temperature Conditions near the Bottom of Well IDDP-1 in Krafla, Northeast Iceland, *Geothermics*, 49, (2014), 49–57.

Bertani, R., Büsing, H., Buske, S., Dini, A., Hjelstuen, M., Luchini, M. and Manzella, A.: The First Results of the DESCRAMBLE Project, *43rd Workshop on Geothermal Reservoir Engineering*, Stanford University, (2018), 1–16

Bu, X., Ma, W. and Li, H.: Geothermal Energy Production Utilizing Abandoned Oil and Gas Wells, *Renewable Energy*, 41, (2012), 80–85.

Caulk, R. A., and Tomac., I.: Reuse of Abandoned Oil and Gas Wells for Geothermal Energy Production, *Renewable Energy*, 112, (2017), 388–97.

Cheng, W., Li,T. , Nian, Y. and Wang, C.: Studies on Geothermal Power Generation Using Abandoned Oil Wells, *Energy*, 59, (2013), 248–54.

Dijkshoorn, L., Speer, S., and Pechnig, R.: Measurements and Design Calculations for a Deep Coaxial Borehole Heat Exchanger in Aachen, Germany, *International Journal of Geophysics*, (2013).

Grigoli, F., Cesca, S., Rinaldi, A.P., Manconi, A. , Lopez-Comino, J.A., Clinton, J.F., Westaway, R., Cauzzi, C., Dahm, T., and Wiemer, S.: The November 2017 Mw 5.5 Pohang Earthquake: A Possible Case of Induced Seismicity in South Korea, *Science*, (2018).

Falcone, G., Liu, X., Okech, R.R., Seyidov, F. and Teodoriu, C.: Assessment of Deep Geothermal Energy Exploitation Methods: The Need for Novel Single-Well Solutions, *Energy*, 160, (2018), 54–63.

Frideifsson, G. O., Palsson, B. Albertsson, A. L., Stefansson, B. Gunnlaugsson, E., Ketilsson, J., and Gislason., P.: IDDP-1 Drilled Into Magma - World's First Magma-EGS System Created, *World Geothermal Congress 2015*, (2015), 12.

Fuss, S., Szolgayova, J., Obersteiner, M., and Gusti.. M.: Investment under Market and Climate Policy Uncertainty, *Applied Energy*, 85, (2008), 708–21.

Holmberg, H., Acuña, J., Næss, E, and Sønju, O.K.: Thermal Evaluation of Coaxial Deep Borehole Heat Exchangers, *Renewable Energy*, 97, (2016), 65–76.

Huang, X., Zhu, J. and Li. J. : On Wellbore Heat Transfer and Fluid Flow in the Doublet of Enhanced Geothermal System, *Energy Procedia* 75, (2015), 946–55.

Ingason, K, Kristjánsson,V. and Einarsson., K.: Design and Development of the Discharge System of IDDP-1. *Geothermics*, 49, (2014), 58–65.

Kohl, T., Brenni,R. and Eugester, W.: System Performance of a Deep Borehole Heat Exchanger, *Geothermics*, 31, (2002), 687–708.

Kohl, T., Salton, M. and Rybach, L.:Data Analysis of the Deep Borehole Heat Exchanger Plant Weissbad (Switzerland), *World Geothermal Congress 2000*, (2000), 2671–76.

Kolo, I., Sousa,R. and Zhang,T.: Heat Transmission in a Geothermal Wellbore : Modelling and Application, *19th Australasian Fluid Mechanics Conference*, Melbourne, Australia, (2014).

Kujawa, T., Nowak, W. and Stachel., A.A.: Utilization of Existing Deep Geological Wells for Acquisitions of Geothermal Energy, *Energy* ,31 ,(2006), 650–64.

Morita, K., Bollmeier, W. S., and Mizogami, H.: An Experiment to Prove the Concept of the Downhole Coaxial Heat Exchanger (DCHE) in Hawaii (1992).

Noorollahi, Y., Pourarshad, M., Jalilinasrabady,S. and Yousefi, H.: Numerical Simulation of Power Production from Abandoned Oil Wells in Ahwaz Oil Field in Southern Iran, *Geothermics*, 55, (2015), 16–23.

Palsson, B, Holmgeirsson, S., Gudmundsson,A., Boasson, H. A., Ingason, K., Sverrisson, H. and Thorhallsson, S.: Drilling of the Well IDDP-1, *Geothermics*, 49, (2014), 23–30.

Schiffman, P., Zierenberg, R. A., Mortensen, A. K., Fridleifsson, G. Ó and Elders, W. A.: High Temperature Metamorphism in the Conductive Boundary Layer Adjacent to a Rhyolite Intrusion in the Krafla Geothermal System, Iceland, *Geothermics*, 49, (2014), 42–48

Scott, S., Driesner, T. and Weis., P.: Hydrology of a Supercritical Flow Zone Near a Magmatic Intrusion in the IDDP-1 Well–Insights from Numerical Modeling, *World Geothermal Congress 2015* 2(2015), 5.

Table 4: Parameters of the materials used in the CFD model

Properties from Kohl et al. 2000	ρ [kg/m³]	k [W/m.K]	c [J/kg.K]	DBHE Design	1	2	
Water	998.2	0.6	4182	Depth [m]	2008-2070	2069-2070	
Casing	7848	46.9	3500	Cell number	418000	424800	
Cement	3150	3	2000				
Basalt (Axelsson et al. 2014)	2700	2.5	800	Zone	1	2	3
Insulated layer (Axelsson et al. 2014)	2700	1.5	800	Porosity [%]	1	10	1
External Wall properties				Permeability [m²]	10^{-20}	10^{-14} (Scott et al. 2015)	10^{-20}
0-27 [m]	3000	0.08	2105				
27-198 [m]	3000	1	2420				
198-364 [m]	3000	2.41	2540				
364-801 [m]	3000	46.96	3500				
801-916 [m]	3000	0.7	2225				
916-1213 [m]	3000	43.043	3500				
Insulated wall (Noorollahi et al. 2015)	3000	0.027	2540				

Table 5: Equations for the axis and radial momentum in axis in an axisymmetric domain

Axis momentum [3]	$\frac{\partial(\rho v_x)}{\partial t}+\frac{1}{r}\frac{\partial(r\rho v_x v_x)}{\partial x}+\frac{1}{r}\frac{\partial(r\rho v_r v_x)}{\partial r}=-\frac{\partial\rho}{\partial x}+\frac{1}{r}\frac{\partial[r\mu(2\frac{\partial v_x}{\partial x})-\frac{2}{3}(\nabla.\vec{v})]}{\partial x}+\frac{1}{r}\frac{\partial[r\mu\frac{\partial v_x}{\partial r}+\frac{\partial v_r}{\partial x}]}{\partial r}+\rho\vec{g}$
Radial momentum [4]	$\frac{\partial(\rho v_r)}{\partial t}+\frac{1}{r}\frac{\partial(r\rho v_x v_r)}{\partial x}+\frac{1}{r}\frac{\partial(r\rho v_r v_r)}{\partial r}=-\frac{\partial\rho}{\partial r}+\frac{1}{r}\frac{\partial[r\mu(\frac{\partial v_r}{\partial x}+\frac{\partial v_x}{\partial r})]}{\partial x}+\frac{1}{r}\frac{\partial[r\mu(2\frac{\partial v_r}{\partial r}-\frac{2}{3}(\nabla.\vec{v})]}{\partial r}-2\mu\frac{v_r}{r}+\frac{2}{3}\frac{\mu}{r}(\nabla.\vec{v})$

Where $\nabla.\vec{v}=\frac{\partial v_r}{\partial r}+\frac{v_r}{r}$ [5] (ANSYS 2016)